



UNIVERSITÀ DI PARMA

ARCHIVIO DELLA RICERCA

University of Parma Research Repository

Formation of the Huajiang Grand Canyon (southwestern China) driven by the evolution of a Late Pleistocene tiankeng

This is the peer reviewed version of the following article:

Original

Formation of the Huajiang Grand Canyon (southwestern China) driven by the evolution of a Late Pleistocene tiankeng / Fan, Yunlong; Columbu, Andrea; Xiong, Kangning; Luo, Guangjie; Li, Song; Wang &, Xuefeng; Wu, Yangyang. - In: ACTA GEOCHIMICA. - ISSN 2365-7499. - (2022).

Availability:

This version is available at: 11381/2914770 since: 2022-05-02T11:56:50Z

Publisher:

Published

DOI:

Terms of use:

Anyone can freely access the full text of works made available as "Open Access". Works made available

Publisher copyright

note finali coverpage

(Article begins on next page)

02 May 2026

Metadata of the article that will be visualized in OnlineFirst

ArticleTitle	Formation of the Huajiang Grand Canyon (southwestern China) driven by the evolution of a Late Pleistocene tiankeng	
--------------	--	--

Article Sub-Title		
-------------------	--	--

Article CopyRight	The Author(s), under exclusive licence to Science Press and Institute of Geochemistry, CAS and Springer-Verlag GmbH Germany, part of Springer Nature (This will be the copyright line in the final PDF)	
-------------------	--	--

Journal Name	Acta Geochimica	
--------------	-----------------	--

Corresponding Author	FamilyName	Fan
	Particle	
	Given Name	Yunlong
	Suffix	
	Division	Key Laboratory of Western China's Environmental Systems (Ministry of Education), College of Earth and Environmental Sciences
	Organization	Lanzhou University
	Address	Lanzhou, 730000, Gansu, China
	Division	Guizhou Provincial Key Laboratory of Geographic State Monitoring of Watershed, School of Geography and Resource Science
	Organization	Guizhou Education University
	Address	Guiyang, 550018, Guizhou, China
	Phone	
	Fax	
	Email	fany114@lzu.edu.cn

Corresponding Author	FamilyName	Xiong
	Particle	
	Given Name	Kangning
	Suffix	
	Division	School of Karst Science
	Organization	Guizhou Normal University
	Address	Guiyang, 550001, Guizhou, China
	Phone	
	Fax	
	Email	xiongkn@163.com
	URL	
	ORCID	

Author	FamilyName	Columbu
	Particle	
	Given Name	Andrea
	Suffix	
	Division	Department of Chemistry, Life Sciences and Environmental Sustainability
	Organization	University of Parma
	Address	43124, Parma, Italy
	Phone	
	Fax	
	Email	
	URL	
	ORCID	

Author	FamilyName Particle Given Name Suffix Division Organization Address Phone Fax Email URL ORCID	Luo Guangjie Guizhou Provincial Key Laboratory of Geographic State Monitoring of Watershed, School of Geography and Resource Science Guizhou Education University Guiyang, 550018, Guizhou, China
Author	FamilyName Particle Given Name Suffix Division Organization Address Phone Fax Email URL ORCID	Li Song Guizhou Provincial Key Laboratory of Geographic State Monitoring of Watershed, School of Geography and Resource Science Guizhou Education University Guiyang, 550018, Guizhou, China
Author	FamilyName Particle Given Name Suffix Division Organization Address Phone Fax Email URL ORCID	Wang Xuefeng Key Laboratory of Cenozoic Geology and Environment, Institute of Geology and Geophysics Chinese Academy of Sciences Beijing, 100029, China
Author	FamilyName Particle Given Name Suffix Division Organization Address Phone Fax Email URL ORCID	Wu Yangyang Guizhou Provincial Key Laboratory of Geographic State Monitoring of Watershed, School of Geography and Resource Science Guizhou Education University Guiyang, 550018, Guizhou, China
Schedule	Received Revised Accepted	9 Sep 2021 28 Oct 2021 31 Oct 2021
Abstract	Collapse is a common geomorphic process in karst areas, especially on the Yunnan-Guizhou Plateau, which has a tectonic background of integral uplift. The frequent occurrence of collapse processes in karst underground caves and canyons indicates that collapses play an important role in the formation of canyons. Through an analysis of the morphology of a semicircular cliff in the Huajiang Grand Canyon and an investigation of sediments at the bottom of the cliff, a large-scale collapse event was found to have occurred. U-series dating of secondary calcium carbonate cement in the collapse breccias indicates that collapse processes occurred approximately 200 ka. According to the geomorphological evolution of the Huajiang Grand Canyon, the following geomorphic evolutionary process is proposed: underground river—cave hall—collapse of a tiangkeng—tiangkeng degradation—canyon formation. These findings also show that the dating of collapsed breccia cement can be effectively used to determine the development times of karst canyons and the formation ages of tiangkengs.	



2 **Formation of the Huajiang Grand Canyon (southwestern China)**
3 **driven by the evolution of a Late Pleistocene tiankeng**

4 Yunlong Fan^{1,2} · Andrea Columbu³ · Kangning Xiong⁴ · Guangjie Luo² ·
5 Song Li² · Xuefeng Wang⁵ · Yangyang Wu²

6 Received: 9 September 2021 / Revised: 28 October 2021 / Accepted: 31 October 2021
7 © The Author(s), under exclusive licence to Science Press and Institute of Geochemistry, CAS and Springer-Verlag GmbH Germany, part of
8 Springer Nature 2021

9 **Abstract** Collapse is a common geomorphic process in
10 karst areas, especially on the Yunnan-Guizhou Plateau,
11 which has a tectonic background of integral uplift. The
12 frequent occurrence of collapse processes in karst under-
13 ground caves and canyons indicates that collapses play an
14 important role in the formation of canyons. Through an
15 analysis of the morphology of a semicircular cliff in the
16 Huajiang Grand Canyon and an investigation of sediments
17 at the bottom of the cliff, a large-scale collapse event was
18 found to have occurred. U-series dating of secondary cal-
19 cium carbonate cement in the collapse breccias indicates
20 that collapse processes occurred approximately 200 ka.
21 According to the geomorphological evolution of the Hua-
22 jiang Grand Canyon, the following geomorphic

evolutionary process is proposed: underground river—cave 23
hall—collapse of a tiankeng—tiankeng degradation—can- 24
yon formation. These findings also show that the dating of 25
collapsed breccia cement can be effectively used to 26
determine the development times of karst canyons and the 27
formation ages of tiankengs. **AQ1** 28

29 **1 Introduction**

30 Canyons are peculiar landscape morphologies produced by 30
multiple processes (Hill et al. 2008; Karlstrom et al. 2014; 31
Wang et al. 2014). Canyons form in different lithologies, 32
but they are often found in karst terrains (Ford 1973; 33
Abbott et al. 2015; Telbiszet al. 2019). Because karst 34
allows underground drainage, river banks are not signifi- 35
cantly eroded, and steep slopes are preserved. Therefore, 36
deep canyons are a common and remarkable feature of 37
karstic landscapes (Sweeting 1995). In uplifting areas, 38
rivers progressively cut across landforms (Nicod 1997); 39
thus, the development of deep canyons is controlled by the 40
base level (Fabre and Nicod 1978). Another key factor in 41
the development of canyons is gradually deepening from 42
the lower to upper reaches of valleys, which is driven by 43
the migration of the knickpoint (Germanoski and Ritter 44
1988; Hu et al. 2016). However, in karst terrains, cave 45
collapse also plays a significant role (Nicod 1997). 46

47 The Yunnan–Guizhou Plateau (Southwest China) has
48 been uplifted since the Cenozoic (Tapponnier 2001; Clark
49 et al. 2006) due to the uplift of the Qinghai–Tibetan Pla-
50 teau. The rapid uplift of this extensive Chinese karst region
51 has favoured underground drainage and thus the formation
52 of caves. The expansion of underground spaces (lateral
53 and/or vertical expansion) eventually leads to the collapse

A1 ✉ Yunlong Fan
A2 fanyl14@lzu.edu.cn

A3 ✉ Kangning Xiong
A4 xiongkn@163.com

A5 ¹ Key Laboratory of Western China's Environmental Systems
A6 (Ministry of Education), College of Earth and Environmental
A7 Sciences, Lanzhou University, Lanzhou 730000, Gansu,
A8 China

A9 ² Guizhou Provincial Key Laboratory of Geographic State
A10 Monitoring of Watershed, School of Geography and
A11 Resource Science, Guizhou Education University,
A12 Guiyang 550018, Guizhou, China

A13 ³ Department of Chemistry, Life Sciences and Environmental
A14 Sustainability, University of Parma, 43124 Parma, Italy

A15 ⁴ School of Karst Science, Guizhou Normal University,
A16 Guiyang 550001, Guizhou, China

A17 ⁵ Key Laboratory of Cenozoic Geology and Environment,
A18 Institute of Geology and Geophysics, Chinese Academy of
A19 Sciences, Beijing 100029, China

of caves. On the Guizhou Plateau, the collapse of underground river passages is very common (Zhang and Mo 1982; Sweeting 1995; Szczygiel et al. 2018), often causing the opening of the chamber roof to the ground surface. Several morphologies in this area (i.e., large depressions, canyons, valleys, cones, and tower karst) are attributed to cave collapse (Ambert and Nicod 1981; Alexander 2005), including tiankengs. The latter are giant collapse dolines with continuous precipitous walls (Alexander 2005; Zhu and Chen 2005; Waltham 2015; Michelena 2020). In most cases, the accumulation of colluvium can be observed at the bottom of tiankengs. According to the evolution of similar landforms, large underground rivers are prone to collapse, thus forming tiankengs. The Xingwen Tiankeng group in Sichuan (Waltham 2005), Wulong Tiankeng group in Chongqing (Alexander 2005; Szczygiel et al. 2018), and Leye Tiankeng group in Guangxi (Zhu and Waltham 2005) are other examples of tiankengs. Many tiankengs are also distributed on the tributaries of large rivers on the plateau. For example, the Dacao kou and Xiaocao kou Tiankengs on the Yijie River, which is a tributary of the Wujiang River, and the Jiudongtian Tiankeng on the Liuchong River in the upper reaches of the Wujiang River are narrow, long tiankengs formed by collapsed cave passages (An et al. 2019). These tiankengs represent the embryonic form in the evolution from tiankeng to canyon.

The shape of tiankengs evolves because of the lateral expansion of the walls and collapses. If these karst-related features endure through time, the original morphology is obliterated. Thus, understanding the evolution of a karst area where tiankengs have reached a mature stage might be difficult. As for all morphologies related to underground voids (Sasowsky 1998), determining the age of tiankengs is complicated (Shui et al. 2015). There have been several attempts to determine the chronological evolution of these landforms in China using different approaches. According to geological observations, Zhu and Chen (2005) speculated that most tiankengs in China formed since the Late Pleistocene, while Wei et al. (2019) inferred that Fengjie Tiankeng was formed in the late Middle Pleistocene. Meng et al. (2017) also determined that the exposure age of Dashiwei Tiankeng is at least 100–200 ka BP based on bedrock cosmogenic ^{36}Cl exposure dating. Therefore, more exhaustive information about the age and evolution of these morphologies is needed.

Cave deposits can be dated to infer the ages of caves (Polyak et al. 2008; Granger and Fabel 2012; Anthony 2012; Columbu et al. 2021). Chemically precipitated carbonate (i.e., speleothems) is an ideal candidate because U-series dating of calcite is very efficient (Cheng et al. 2016). Importantly, speleothems are deposited after cave formation (Wang et al. 2004; Columbu et al. 2015) in either

subaerial or submerged conditions (De Waele et al. 2018). Speleothems found at the surface indicate that the original hosting cave has been disrupted (Columbu et al. 2017).

This paper investigates the evolution of the Huajiang Grand Canyon on the Guizhou Plateau in the middle reaches of the Beipan River. Geomorphological observations suggest the presence of a relict tiankeng, and secondary carbonate dating was applied to deposits previously formed in underground environments. Accordingly, this paper aims to reconstruct the genesis of the current canyon relative to the maturation of the relict tiankeng, placing this karst-related process into a congruent geochronological timeframe.

2 Area of study

The Beipan River originates from the eastern part of Yunnan Province and flows from northwest to southeast across the Yunnan–Guizhou Plateau (Fig. 1A–B). Reaching the slopes of Guangxi, this river is 449 km long with a drop of 1982 m, corresponding to an average drop of 4.42‰, and has a catchment area of 25,830 km² (Fan et al. 2018). Wide varieties of rocks are exposed in the basin, including a large number of soluble rocks, such as Devonian, Carboniferous, Permian, Triassic limestone, and dolomite, as well as nonsoluble rocks, such as siltstone and mudstone.

Under the influence of lateral extrusion from the southeastern Qinghai–Tibetan Plateau, the Yunnan–Guizhou Plateau has undergone differential uplift alongside the uplift of the Qinghai–Tibetan Plateau. Low-relief and high-elevation surfaces are broadly distributed, elevation decreases gradually from the northwest to the southeast, and western plateau surfaces with altitudes of 2100–2200 m and eastern plateau surfaces with altitudes of 1300–1400 m are relatively intact (Clark et al. 2006). The valleys of the Beipan River and its tributaries are deep, and the plateau is divided by numerous rivers. The surface has experienced extensive erosion, resulting in a shortage of widespread, continuous Quaternary sediments (Liu et al. 2013).

The Huajiang Canyon is located in the middle reaches of the Beipan River, 5 km upstream from Huajiang village (Fig. 1). Covering a total length of 30 km (Fig. 1C), the canyon coincides with the Zhenfeng Fault. On the western side of the fault, a well-preserved karst plateau surface is maintained, with an average elevation of 1300–1400 m (Fig. 1D). On the eastern side of the fault, the terrain is relatively low with no intact plateau surface, forming a hilly country with an elevation of 500–1000 m. With the fault as the boundary, the lower reaches of the river are open, and the river becomes sluggish, while the upper

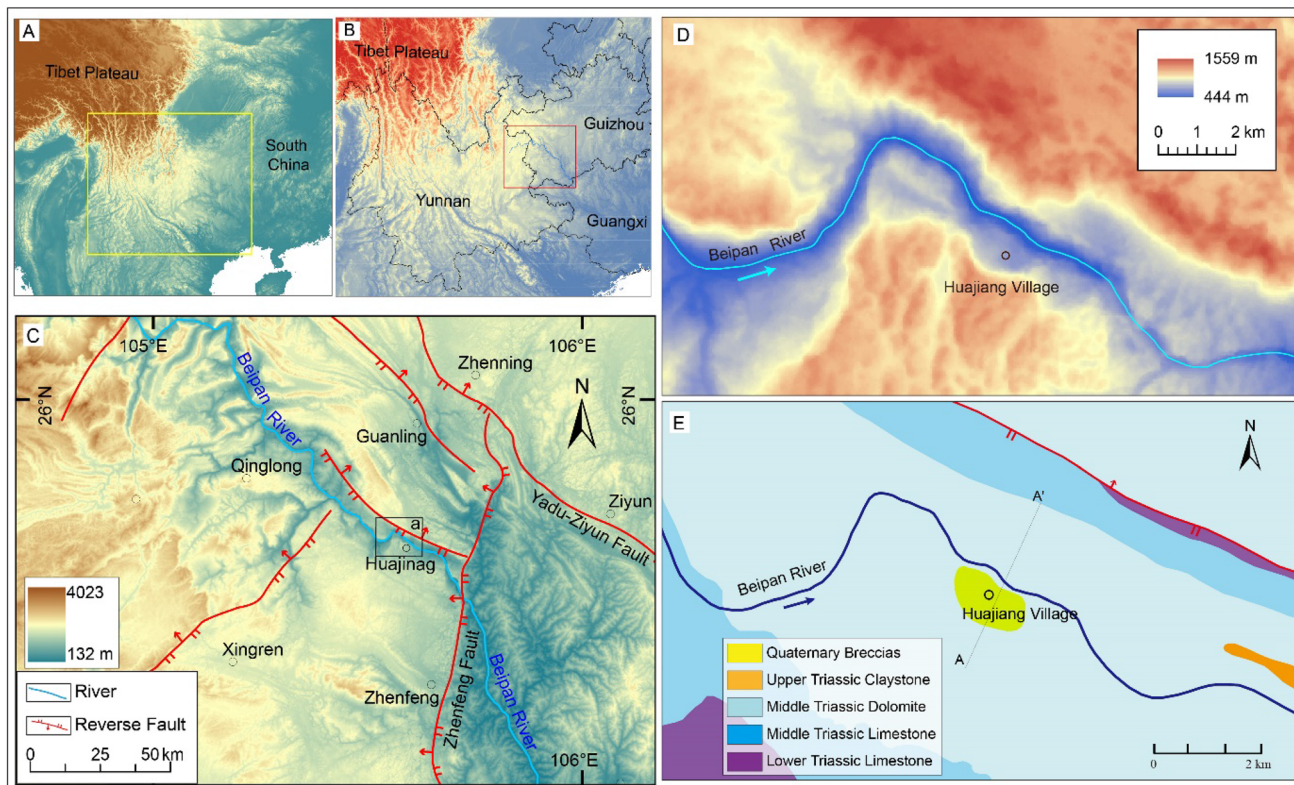


Fig. 1 Study area. **A** Location of the Yunnan–Guizhou Plateau. **B** Location of the Beipan River. **C** Digital elevation model of Huajiang Canyon and surrounding areas, with the main fault system shown. **D** Digital elevation model of the Huajiang Canyon area. **E** Simplified geologic map of Huajiang Canyon (section A–A' is shown in Fig. 3a)

157 reaches exhibit deep canyons. In the section containing
 158 Huajiang village, the vertical drop of the canyon is very
 159 large, with a depth of approximately 800–1000 m. In this
 160 section, the river cuts deeply into the dolomite strata of the
 161 Triassic Yangliujing Formation. In the study area, the
 162 canyons consist of an ~ 3 -km-wide outer canyon and
 163 an ~ 150 -m-wide inner canyon with a depth of 200 m.
 164 The two sides of Huajiang Canyon are surrounded by
 165 plateau surfaces, with several 100–200 m-high fengcongs
 166 present (Fig. 1D).

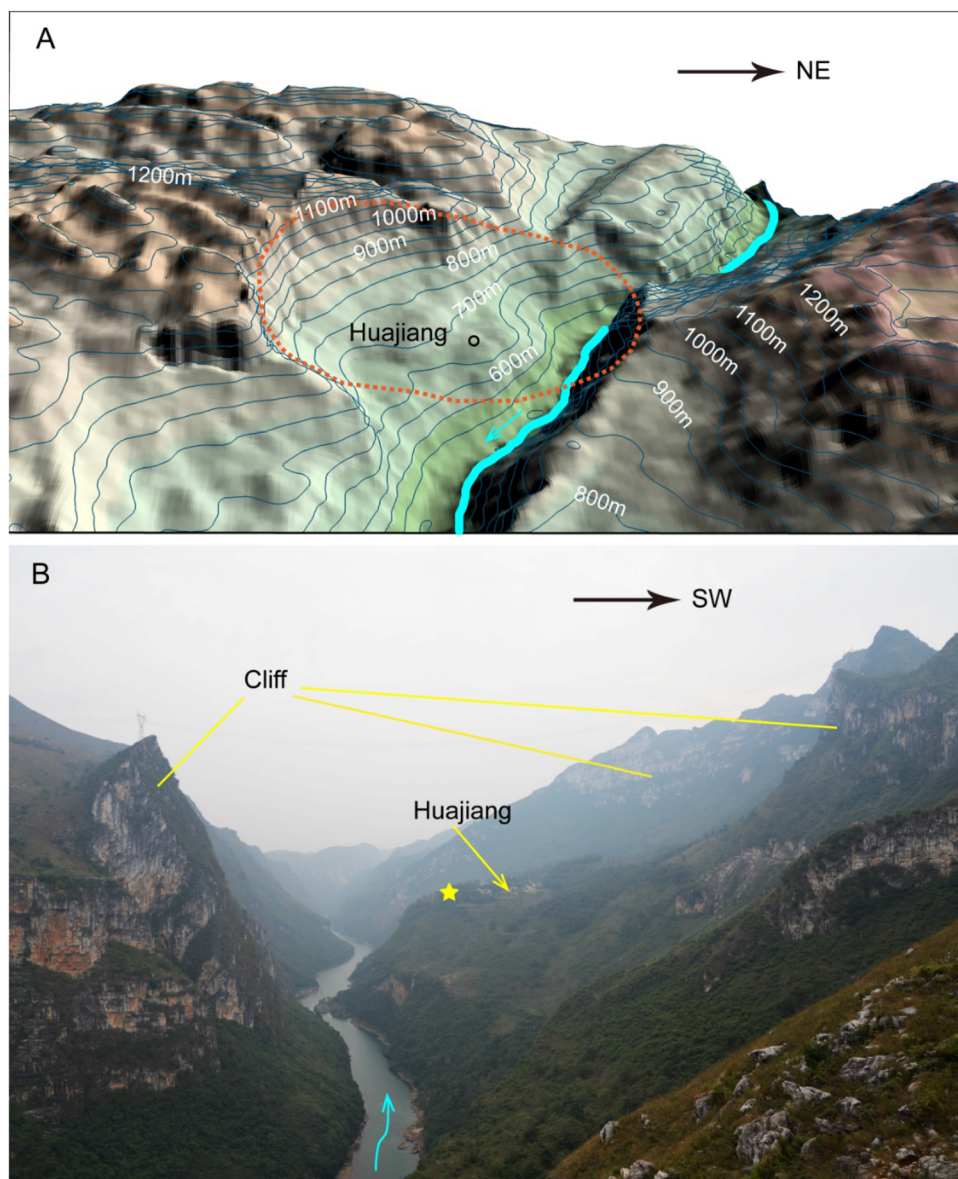
167 Within Huajiang Canyon, a distinct platform is identi-
 168 fied ($25^{\circ}41'52''\text{N}$, $105^{\circ}35'24''\text{E}$). The elevation of this
 169 platform is higher than that of the modern river channel by
 170 approximately 200 m (Fig. 2A). The altitude of the plat-
 171 form is approximately 700 m, and the elevation of the bed
 172 of the Beipan River is 500 m. A semicircular vertical cliff
 173 is retained on the side of the canyon where the Huajiang
 174 platform is located. Furthermore, some residual peaks
 175 occur on the opposite bank of the canyon. A large amount
 176 of karst breccia has been deposited on the platform of
 177 Huajiang village, with a thickness of 5–10 m. The bedrock
 178 beneath the breccias is an ancient cave floor. In addition,
 179 many remains of ancient stalagmites were observed on the
 180 Huajiang platform (Fig. 3).

3 Materials

The breccias on the Huajiang platform are composed of
 dolomites, have a mixed structure with no obvious bed-
 ding, and are densely cemented by secondary calcium
 carbonate (Fig. 3c–j). According to their sedimentary
 characteristics, they can be identified as colluvial breccias
 with a thickness of 5–10 m. Many remains of ancient sta-
 lagmites were observed on the Huajiang platform. Some
 stalagmites remain upright, with dolomite bedrock at the
 bottom (Fig. 3l). Some of the damaged stalagmites are
 buried in the soil (Fig. 3k). Although all of the stalagmites
 were eroded and weathered under the soil in the later stage,
 laminae and morphological characteristics can be identified
 in the fracture section.

Four secondary calcium carbonate deposits on the
 Huajiang platform were investigated (Fig. 3), two of which
 were breccia samples (BHJT2 and BHJT4): BHJT2 located
 at the bottom of the tiankeng (695 m a.s.l.) and BHJT4
 located on the slope at the edge of the tiankeng (780 m
 a.s.l.). The remaining samples (BHJT3BS and BHJT3CS)
 were two ancient stalagmites on the Huajiang platform.
 Samples for dating were obtained from the top and bottom
 of each stalagmite. Fortunately, freshly exposed breccias

Fig. 2 **A** 3D topographic map of Huajiang Canyon. The orange dotted line indicates the shape of the original tiangkeng. **B** Photo of the degraded Huajiang Tiangkeng, looking southeast. The yellow lines point to the remaining cliffs from the collapse



204 could be observed in a slope section excavated during the
 205 construction of a road leading to Huajiang village. The
 206 breccias were well cemented and compact. Sample BHJT2
 207 was collected beside the road (695 m a.s.l.) from a location
 208 1.8 m below the top surface of the breccias. Sample BHJT4
 209 was collected beside the road (780 m a.s.l.) from a location
 210 3 m below the top of the profile. Sampling targeted loca-
 211 tions potentially repaired after post-depositional weather-
 212 ing. Samples were detached from the original surface using
 213 a hammer and chisel. Thin sections of all breccia samples
 214 were prepared for petrographic investigation (Fig. 3f, g–i,
 215 j).

4 Methods

216
 217 Petrographic thin sections were investigated using a Leica
 218 DM4500P polarizing microscope. Subsamples weighing
 219 approximately 50–100 mg were collected for U–Th dating
 220 by drilling along the growth layers using a dental hand
 221 drill. Dating was performed to attempt to establish the ages
 222 of the stalagmites and colluvium cementation to constrain
 223 the time(s) of the collapse event(s). When the bottom or top
 224 of a stalagmite was considered unsuitable for dating due to
 225 obvious clastic material in the laminae, samples of the
 226 closest clean and unaltered calcite were collected.

227 The uranium-series dating method is an effective dating
 228 method for determining geological age based on the dise-
 229 quilibrium between radionuclide ^{238}U and its decay
 230 daughters ^{234}U and ^{230}Th (Edwards et al. 1987). Using

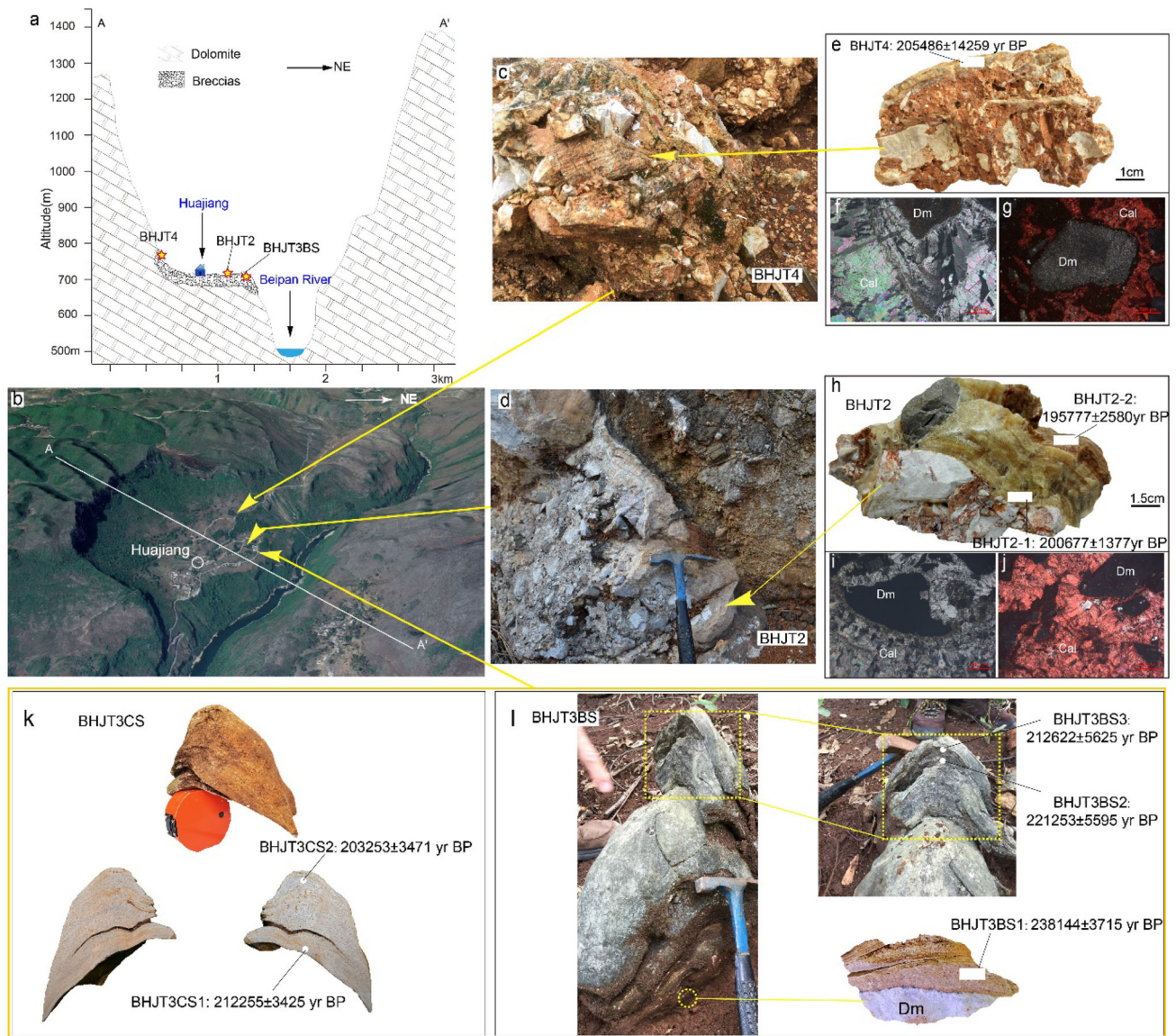


Fig. 3 **a** Huajiang Tiankeng profile. Its position is coincident with the dashed line (A–A′) in Fig. 1E. The yellow stars indicate sampling locations. **b** Satellite image (from Google Earth) showing the degraded Huajiang Tiankeng. The yellow arrows indicate the sampling locations. **c** Karst breccias (BHJT4) deposited in the slope area at the edge of the Huajiang Tiankeng. **d** Karst breccias (BHJT2), deposited at the bottom of the Huajiang Tiankeng. **e** Hand specimen, BHJT4. **f–g** Microphotographs of BHJT4. **h** Hand specimen, BHJT2. **i–j** Microphotographs of BHJT2. **k** Stalagmite buried under the soil and its longitudinal section. Crack formation due to dissolution under the soil is visible in the longitudinal section of the stalagmite. **l** Stalagmites exposed on the Earth’s surface and their ages (the stalagmites are grown on the dolomite bedrock, and samples for dating were collected from the bottom of the stalagmites). The locations of these residual stalagmites **k–l** are shown by yellow stars in Fig. 2B (Dm represents dolomite, and Cal represents calcite)

231 multicollector–inductively coupled plasma–mass spec-
 232 trometry (MC–ICP–MS), the U–Th dating method provides
 233 a dating range from decades to 640 ka (Cheng, 2013). U–
 234 Th dating was performed at the Uranium Series Chronol-
 235 ogy Laboratory of the Institute of Geology and Geophysics
 236 at the Chinese Academy of Sciences in Beijing. Chemical
 237 treatment was performed following the Edwards method
 238 (Edwards et al. 1987; Wang et al. 2017). The subsamples
 239 were first dissolved in HNO₃, followed by the addition of a

few drops of HClO₄. All samples were spiked with a 240
²²⁹Th–²³³U–²³⁶U tracer (Chen et al. 1986; Shen et al. 2002;
 241 Cheng et al. 2013). The mixed solutions were placed on a
 242 150 °C hot plate for 5–10 h and evaporated to dryness.
 243 Then, the samples were dissolved in 2 M HCl and trans-
 244 ferred to clean centrifuge tubes. Approximately 10 mg of
 245 FeCl₃ was added and mixed, followed by a few drops of
 246 NH₃·H₂O to adjust the pH to 7–8. In this step, a slightly
 247 reddish-brown Fe(OH)₃ precipitate was formed, with
 248

249 simultaneous coprecipitation of U and Th from the mixed
 250 liquids. The precipitates were washed twice with ultrapure
 251 water, dissolved in 0.5 mL 7 M HNO₃, and dried again at
 252 150 °C. Then, the samples were dissolved in 7 M HNO₃
 253 and loaded onto 7 M HNO₃-conditioned anion-exchange
 254 columns. Trace metal elements were eluted with 7 M
 255 HNO₃, Th was eluted with 8 M HCl, and U was eluted with
 256 0.1% HNO₃. The U and Th fractions were dried at 150 °C
 257 and dissolved in 2% HNO₃ + 0.1% HF. The U and Th
 258 recovery in this procedure was higher than 90%. The half-
 259 lives of ²³⁴U and ²³⁰Th were determined based on data
 260 proposed by Cheng et al. (2013). MC-ICP-MS was used to
 261 determine the ²³⁰Th age of the eight samples. The details of
 262 the instrumental parameters were described by Wang et al.
 263 (2016).

264 5 Results

265 Petrographic investigations of two breccia hand specimens
 266 facilitated the discrimination of textures and fabrics in each
 267 sample (Fig. 3). All thin sections of breccia samples
 268 showed no traces of dissolution or redeposition and were
 269 thus considered suitable materials for U–Th dating.

270 The results of ²³⁰Th/U dating are presented in Table 1.
 271 In general, the secondary calcium carbonate ages produced
 272 realistic radiometric ages, with samples possessing high
 273 ²³⁸U contents and mostly high ²³⁰Th/²³²Th activity ratios.
 274 Although the ²³²Th content in BHJT4 was high, which may
 275 have been caused by detrital contamination, the
 276 ²³⁰Th/²³²Th ratio was still greater than 20. Accordingly, the
 277 obtained ages have moderate to low uncertainties. For the
 278 breccia samples, the BHJT2-1 age was 200,677 ± 1377 a,
 279 the BHJT2-2 age was 19,577 ± 2580 a, and the BHJT4 age
 280 was 205,486 ± 14,259 a (Fig. 3e–h). The age of the bot-
 281 tom of the BHJT3BS stalagmite was 238,144 ± 3715 a,
 282 while the ages at the top were 221,253 ± 5595 a
 283 (BHJT3BS2) and 212,622 ± 5625 a (BHJT3BS3)
 284 (Fig. 3l). The ages of stalagmite BHJT3CS ranged from
 285 212,255 ± 3425 a (BHJT3CS1) to 203,253 ± 3471 a
 286 (BHJT3CS2) (Fig. 3k).

287 6 Discussion

288 6.1 Age of the colluvium

289 When the underground river was at the elevation of the
 290 platform of Huajiang village, the river eroded the tunnel
 291 laterally, continuously expanding the underground cave
 292 chamber, which provided storage space for large-scale and
 293 possibly multiple collapses. Eventually, a large number of
 294 colluvial deposits accumulated at the bottom of the original

295 underground river channel. Due to the loose structure of
 296 breccia, cementation can occur if infiltrating water is
 297 supersaturated concerning carbonate (Piccini et al. 2003).
 298 Thick secondary calcium carbonate deposits were formed
 299 in some fractures, and these deposits have laminae similar
 300 to cave flowstones (Fig. 3d–h). According to the dates
 301 provided, cementation was probably completed within a
 302 very short time after the collapse (approximately 200 ka).
 303 Because of case hardening, the interblock porosity of the
 304 breccia was reduced, significantly lowering the possibility
 305 of later dissolution (Ford and Williams 2007). Therefore,
 306 the secondary calcium carbonate deposits in the breccia
 307 fractures were probably not redeposited. The lack of
 308 redissolution/redeposition effects promoted a closed sys-
 309 tem for uranium, facilitating reliable U-series dating. The
 310 cementation time of the breccia represents the time of the
 311 collapse event. Stalagmites are products of caves; there-
 312 fore, the ages of the stalagmites indicate when Huajiang
 313 Canyon was still in a cave environment. Karst areas in
 314 Southwest China generally lack sufficient surface sedi-
 315 ments (Liu et al. 2013). Consequently, the evolutionary
 316 history of the Guizhou Plateau is not clear, which greatly
 317 restricts our understanding of the formation and evolu-
 318 tionary processes of the Guizhou karst landforms. This
 319 study attempted to overcome this limitation by determining
 320 the cementation age of karst breccia cement.

321 6.2 Causes of cave collapse in the Huajiang Grand 322 Canyon

323 Geomorphological observations and the presence of
 324 extensive breccia deposits suggest the occurrence of a
 325 large-scale collapse in Huajiang Canyon related to previous
 326 subterranean karst drainage. The stability of caves is lim-
 327 ited (Ford and Williams 2007), especially in areas char-
 328 acterized by rapid tectonic uplift. When the cavern in the
 329 study location was enlarged to a certain volume, it began to
 330 gradually collapse, exposing the underground features at
 331 the surface. Stalagmite BHJT3BS, which is currently at the
 332 surface, clearly supports this scenario. When the tianheng
 333 first formed, it was likely ring-shaped. Its original mor-
 334 phology was eventually obliterated by additional collapses.
 335 At present, a residual vertical cliff remains on the western
 336 side of Huajiang gorge (Fig. 2).

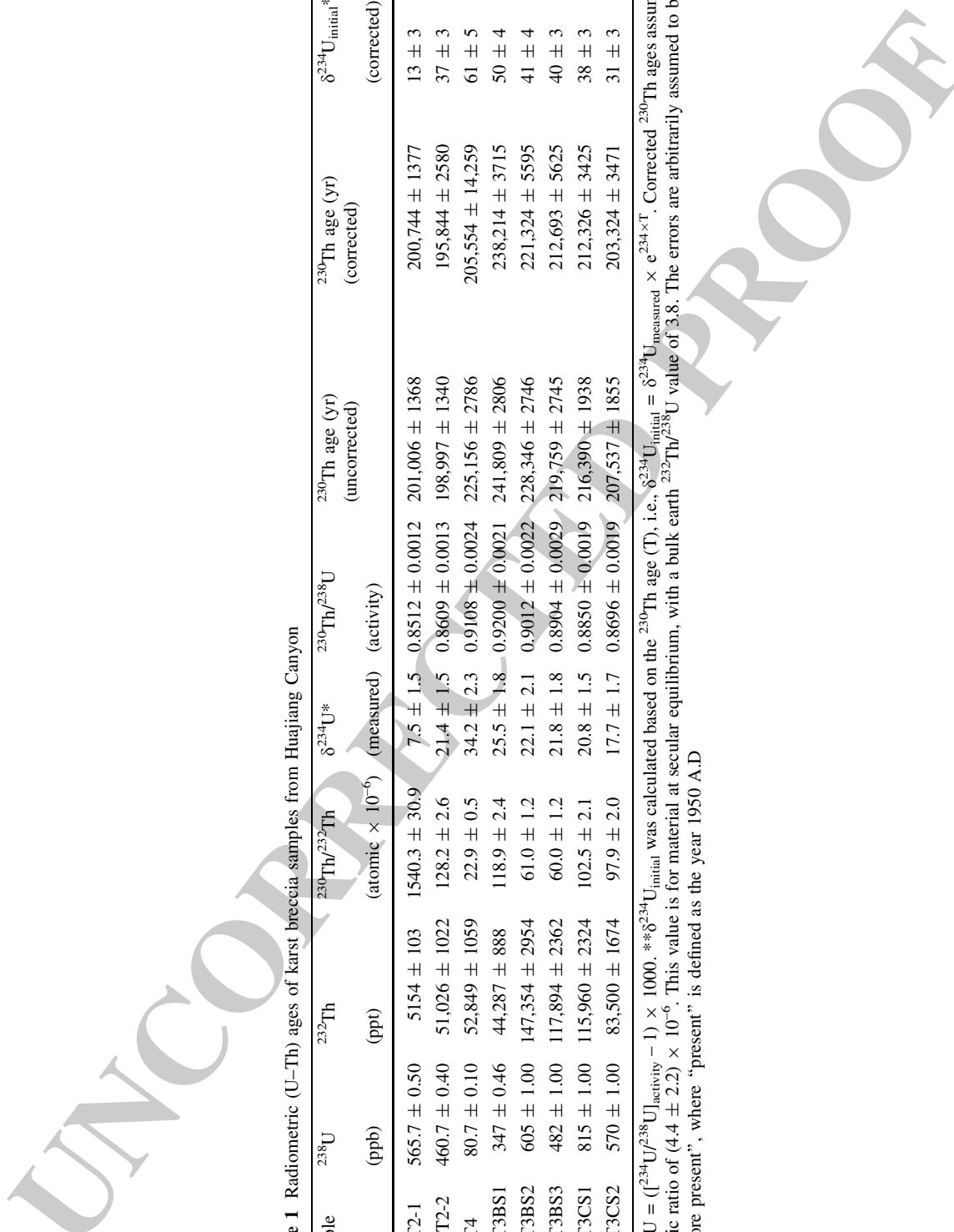
337 Cave collapse in the Huajiang Grand Canyon was pos-
 338 sibly triggered by a combination of the following tectonic
 339 and geological characteristics of the area:

- 340 • Rapid uplift of the Yunnan–Guizhou Plateau since the
 341 Cenozoic is related to the tectonics of the Qinghai–
 342 Tibetan Plateau, which has been in an overall uplift
 343 tectonic environment. This has caused ongoing base
 344 level deepening, which promotes the formation of

Table 1 Radiometric (U–Th) ages of karst breccia samples from Huajiang Canyon

Sample	²³⁸ U (ppb)	²³² Th (ppt)	²³⁰ Th/ ²³² Th (atomic × 10 ⁻⁶)	$\delta^{234}\text{U}^*$ (measured)	²³⁰ Th/ ²³⁸ U (activity)	²³⁰ Th age (yr) (uncorrected)	²³⁰ Th age (yr) (corrected)	$\delta^{234}\text{U}_{\text{initial}}^{***}$ (corrected)	²³⁰ Th age (yr BP) ^{***} (corrected)
BHJT2-1	565.7 ± 0.50	5154 ± 103	1540.3 ± 30.9	7.5 ± 1.5	0.8512 ± 0.0012	201,006 ± 1368	200,744 ± 1377	13 ± 3	200,677 ± 1377
BHJ T2-2	460.7 ± 0.40	51,026 ± 1022	128.2 ± 2.6	21.4 ± 1.5	0.8609 ± 0.0013	198,997 ± 1340	195,844 ± 2580	37 ± 3	195,777 ± 2580
BHJT4	80.7 ± 0.10	52,849 ± 1059	22.9 ± 0.5	34.2 ± 2.3	0.9108 ± 0.0024	225,156 ± 2786	205,554 ± 14,259	61 ± 5	205,486 ± 14,259
BHJT3BS1	347 ± 0.46	44,287 ± 888	118.9 ± 2.4	25.5 ± 1.8	0.9200 ± 0.0021	241,809 ± 2806	238,214 ± 3715	50 ± 4	238,144 ± 3715
BHJT3BS2	605 ± 1.00	147,354 ± 2954	61.0 ± 1.2	22.1 ± 2.1	0.9012 ± 0.0022	228,346 ± 2746	221,324 ± 5595	41 ± 4	221,253 ± 5595
BHJT3BS3	482 ± 1.00	117,894 ± 2362	60.0 ± 1.2	21.8 ± 1.8	0.8904 ± 0.0029	219,759 ± 2745	212,693 ± 5625	40 ± 3	212,622 ± 5625
BHJT3CS1	815 ± 1.00	115,960 ± 2324	102.5 ± 2.1	20.8 ± 1.5	0.8850 ± 0.0019	216,390 ± 1938	212,326 ± 3425	38 ± 3	212,255 ± 3425
BHJT3CS2	570 ± 1.00	83,500 ± 1674	97.9 ± 2.0	17.7 ± 1.7	0.8696 ± 0.0019	207,537 ± 1855	203,324 ± 3471	31 ± 3	203,253 ± 3471

* $\delta^{234}\text{U} = \left(\frac{^{234}\text{U}/^{238}\text{U}}{\text{activity} - 1} \right) \times 1000$. ** $\delta^{234}\text{U}_{\text{initial}}$ was calculated based on the ²³⁰Th age (T), i.e., $\delta^{234}\text{U}_{\text{initial}} = \delta^{234}\text{U}_{\text{measured}} \times e^{234 \times T}$. Corrected ²³⁰Th ages assume an initial ²³⁰Th/²³²Th atomic ratio of (4.4 ± 2.2) × 10⁻⁶. This value is for material at secular equilibrium, with a bulk earth ²³²Th/²³⁸U value of 3.8. The errors are arbitrarily assumed to be 50%. ***B.P. denotes “before present”, where “present” is defined as the year 1950 A.D.



345 underground rivers (Sweeting 1995). The Huajiang
346 Grand Canyon is located west of the Zhenfeng thrust
347 fault. The western side is the hanging wall of the thrust
348 fault, and its tectonic uplift significantly increases the
349 river drop on both sides of the fault, resulting in
350 accelerated river downcutting.

351 • From a geological perspective, the Huajiang Grand
352 Canyon is carved into dolomite. In the past, the
353 dissolution rate of dolomite was believed to be lower
354 than that of limestone. However, a recent study on the
355 chemical denudation rate of dolomite in the Shibing
356 area of Guizhou Province showed that the dolomite
357 chemical denudation rate is similar to or even higher
358 than that of limestone under a similar climate (He et al.
359 2018). Importantly, dolomite is prone to collapse if a
360 static equilibrium is compromised (Luo et al. 2019).
361 Therefore, physical collapse is particularly important
362 for the formation of dolomite caves. The platform
363 around Huajiang village is characterized by abundant
364 collapse breccia deposits, which suggest the occurrence
365 of a large-scale collapse event. U-series dating analysis
366 of breccia cement samples from different parts and
367 altitudes in the tiankeng showed that the samples
368 experienced approximately synchronous cementation.
369 This implies that the collapse leading to the formation
370 of the tiankeng was completed in one main event or at
371 least within a short period. There are no younger large-
372 scale colluvial deposits above the breccia, except for
373 recent small-scale colluvial deposits found under the
374 cliff at the Huajiang Tiankeng. Minor collapse pro-
375 cesses may continue, but the collapse event that played
376 a decisive role in the landscape of Huajiang gorge
377 occurred ~ 200 ka. In addition, many ancient stalag-
378 mites were observed on the Huajiang platform (Fig. 3).
379 As stalagmites do not occur at the surface, the
380 development of the gorge can certainly be attributed
381 to cave collapse.

382 6.3 Evolutionary processes of Huajiang Canyon

383 According to field observations during the geomorpho-
384 logical survey and based on chronological data, the
385 development and evolutionary process of Huajiang Canyon
386 can be divided into four stages as follows:

- 387 • During the Early Pleistocene, surface rivers flowed
388 through wide valleys in the Huajiang gorge (Stage 1 in
389 Fig. 4), and the karst system had not yet formed.
390 Previous studies have also indicated the formation of
391 wide valleys in the upper reaches during the early
392 Pleistocene (Li 2001).
393 • Subsequently, due to the tectonic uplift of the western
394 side of the Zhenfeng Fault, the Beipan River base level

395 dropped, promoting underground excavation. The
396 underground river channel likely continued to erode
397 laterally, continuously expanding the tunnel and form-
398 ing large caverns, which favoured the occurrence of
399 collapse and provided storage space for the accumula-
400 tion of colluvium (Stage 2 in Fig. 4). At this stage,
401 stalagmites formed at the bottom of the newly formed
402 caves (Fig. 4). These stalagmites stopped growing
403 approximately 203 ka.

- 404 • The space in the underground cave continuously
405 expanded, leading to one or more collapse events.
406 According to the U-series dating of the cement, some
407 collapses occurred ~ 200 ka BP. Subsequently, the
408 underground rivers were exposed as surface rivers, and
409 colluvium accumulated at the bottom of the tiankeng
410 (Stage 3 in Fig. 4).
411 • After colluvial deposition, with continuous tectonic
412 uplift, the river underwent rapid incision. From the
413 bottom of the colluvium, at altitudes of 685 to 500 m
414 (current height of the river), the incision depth reached
415 185 m, forming a deep canyon (Stage 4 in Fig. 4).
416 Since 200 ka, the river incision rate has reached
417 0.92 m/ka. This result is close to the research result
418 of the incision rate of the Nizhu River canyon in the
419 upper reaches of the Beipan River (Fan et al. 2021).
420 Crustal uplift is a necessary condition for the formation
421 of deep canyons (Hu et al. 2016). Rapid downcutting of
422 the Huajiang gorge by the Beipan River was mainly
423 controlled by the activity of the Zhenfeng Fault, which
424 was attributable to the acceleration of tectonic uplift on
425 the western side of the Zhenfeng Fault.

7 Conclusion 426

427 In this study, the formation and evolutionary processes of
428 Huajiang Grand Canyon were explored. Field surveys were
429 conducted, and analyses of samples collected from Hua-
430 jiang Canyon in the middle reaches of the Beipan River
431 were performed. The main findings can be summarized as
432 follows:

- 433 • A large number of collapsed breccias were preserved
434 on the platform in the residual tiankeng of the Huajiang
435 Grand Canyon on the Beipan River. U-series dating of
436 two stalagmites found at the surface attested to the
437 presence of an underground environment between 238
438 and 203 ka. In contrast, the ages of breccia cements
439 revealed that a large-scale collapse event occurred in
440 Huajiang Grand Canyon at least ~ 200 ka.
441 • Collapse is a very common geomorphic process in karst
442 areas, especially under a tectonic background of
443 integral uplift, such as that of the Yunnan–Guizhou

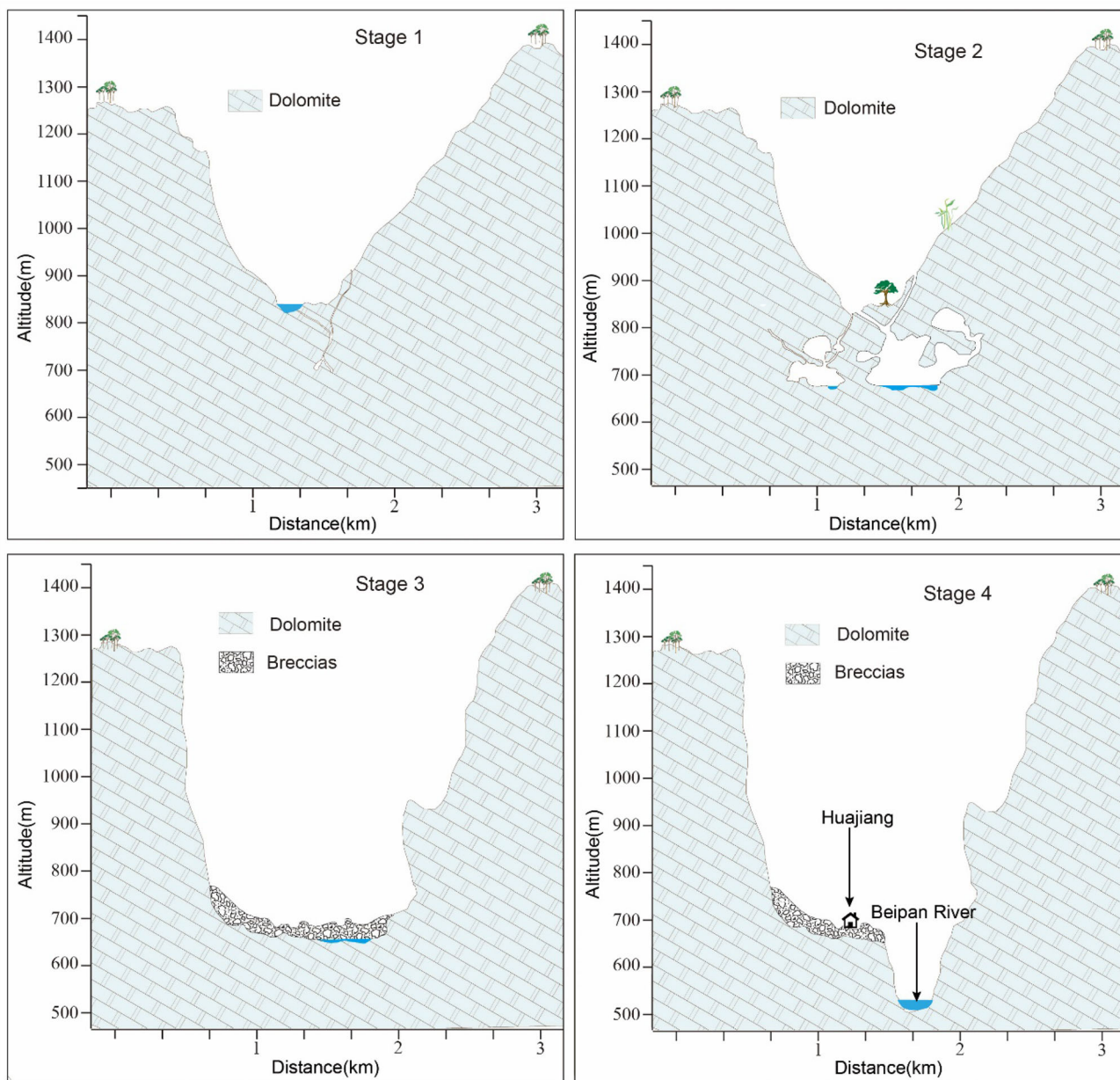


Fig. 4 Evolutionary model of Huajiang Canyon and the Beipan River

444 Plateau. Collapses frequently occur in karst under-
 445 ground caves and canyons. Many cave collapses lead to
 446 the formation of skylights and tiankengs, and contin-
 447 uous collapse leads to the formation of canyons.
 448 Therefore, the collapse process is a common and very
 449 important formation mechanism in the evolution of
 450 karst gorges.

451 • Collapse phenomena and associated colluvium are very
 452 common in karst areas, but their ages of occurrence are
 453 difficult to determine. By U-series chronology testing
 454 of collapse breccia cement, the time of collapse can be
 455 accurately determined. This approach, combined with

456 analyses of cave-specific deposits such as stalagmites,
 457 may provide an effective means for studying canyon
 458 development and determining the ages of tiankeng
 459 formations in karst areas.

460 **Acknowledgements** We thank Ming Tan, Paul W. Williams, Yu Liu,
 461 Changshun Song, Wenlong Zhou, Taiping Ye and Zongmeng Li for
 462 helpful discussions on various aspects of this work. This research was
 463 funded by the National Natural Science Foundation of China
 464 (Grant:42061001, 41501006); The Science and Technology Founda-
 465 tion of Guizhou Province (Grant: Qianke Jichu-ZK[2021]190); Natu-
 466 ral science research funding project of Guizhou Provincial
 467 Department of Education (Grant: Qian Jiao KY[2021]036).



468 Declaration

469 **Conflict of interest** On behalf of all authors, the corresponding
470 author states that there is no conflict of interest.

471 References

- 472 Abbott L, Lundstrom C, Traub C (2015) Rates of river incision and
473 scarp retreat in eastern and central grand canyon over the past
474 half million years: evidence for passage of a transient knickzone.
475 *Geosphere* 11(3):638–659
- 476 Alexander K (2005) Cave un-roofing as a large-scale geomorphic
477 process. *Cave Karst Sci* 32(2–3):93–98
- 478 Ambert P, Nicod J (1981) Sur quelques karsts de Serbie, au voisinage
479 du Danube. Leurs rapports avec l'évolution du bassin pannonien.
480 *Revue Géographique De L'est* 21(4):235–249
- 481 An D, Zhou Z, Xue BQ, Yang E, Fan B, Zhu C et al (2019) Spatial
482 distribution characteristics and the geomorphological evolution
483 process of the Jiudongtian cave system in Guizhou Province.
484 *Carsologica Sinica* 6:967–976
- 485 Anthony D (2012) Multilevel caves and landscape evolution. In:
486 *Encyclopedia of Caves (Second Edition)* pp 528–531
- 487 Chen J, Edwards R, Wasserburg G (1986) ^{238}U , ^{234}U and ^{232}Th in
488 seawater. *Earth Planet Sci Lett* 80(3–4):241–251
- 489 Cheng H, Edwards L SC, Polyak V, Asmerom Y, Woodhead J,
490 Hellstrom J, Wang Y, Kong X, Spötl C, Wang X, Alexander J
491 et al (2013) Improvements in ^{230}Th dating, ^{230}Th and ^{234}U half-
492 life values, and U-Th isotopic measurements by multi-collector
493 inductively coupled plasma mass spectrometry. *Earth Planet Sci
494 Lett* 371–372:82–91
- 495 Cheng H, Edwards R, Sinha A, Christoph S, Liang Y, Shitao C,
496 Megan K, Gayatri K, WX, Li X, Kong X, Wang Y, Ning Y,
497 Zhang H et al (2016) The Asian monsoon over the past 640,000
498 years and ice age terminations. *Nature* 534(7609):640–646
- 499 Clark M, Royden L, Whipple K, Burchfiel B, Zhang X, Tang W et al
500 (2006) Use of a regional, relict landscape to measure vertical
501 deformation of the eastern tibetan plateau. *J Geophys Res Earth
502 Surf* 111:F03002. <https://doi.org/10.1029/2005JF000294>
- 503 Columbu A, Waele J, Forti P, Montagna P, Drysdale R et al (2015)
504 Gypsum caves as indicators of climate-driven river incision and
505 aggradation in a rapidly uplifting region. *Geology*
506 43(6):539–542
- 507 Columbu A, Audra P, Gázquez F, D'Angeli IM, Bigot JY, Koltai G,
508 Chiesa R, Yu TL, Hu HM, Shen CC et al (2021) Hypogenic
509 speleogenesis, late stage epigenic overprinting and condensa-
510 tion-corrosion in a complex cave system in relation to landscape
511 evolution (Toirano, Liguria, Italy). *Geomorphology* 376:107561
- 512 Columbu A, Chiarini V, De Waele J, Drysdale R, Woodhead J,
513 Hellstrom J, Forti P et al (2017) Late quaternary speleogenesis
514 and landscape evolution in the northern Apennine evaporite
515 areas. *Earth Surf Proc Land* 42(10):1447–1459
- 516 De Waele J, D'Angeli IM, Bontognali T, Tuccimei P, Scholz D,
517 Jochum KP, Columbu A, Bernasconi SM, Fornós JJ, González
518 ERG, Tisato N (2018) Speleothems in a north Cuban cave
519 register sea level changes and Pleistocene uplift rates. *Earth Surf
520 Proc Land* 43:2313–2326
- 521 Edwards L, Chen J, Wasserburg G (1987) ^{238}U , ^{234}U , ^{230}Th , ^{232}Th
522 systematics and the precise measurement of time over the past
523 500,000 years. *Earth Planet Sci Lett* 81(2–3):175–192
- 524 Fabre G, Nicod J (1978) Niveaux de base actuels dans les principaux
525 canyons du Languedoc oriental et des Plans de provence. *IJS*
526 10(3):279–291
- Fan YL, Liu JJ, Zhu KW, Li HB, Zou XX (2021) Study on river
527 downcutting rate in Karst Canyon—a case study of Nizhu River
528 Grand Canyon in Beipan River. *Q Sci* 41(6):1558–1564
- 529 Fan YL, Pan BT, Hu ZB, Ren DY, Chen QW, Liu FL, Li ZM (2018)
530 An analysis of tectonic geomorphologic characteristics of the
531 Beipanjiang basin in the Yunnan-Guizhou plateau. *Adv Earth
532 Sci* 33(7):751–761
- 533 Ford D (1973) Development of the canyons of the South Nahanni
534 river NWT. *Canad J Earth Sci* 10(3):366–378
- 535 Ford D, Williams P (2007) Karst hydrogeology and geomorphology.
536 Wiley, Chichester, pp 99–134, 265–270
- 537 Germanoski D, Ritter D (1988) Tributary response to local base level
538 lowering below a dam. *Regul Rivers Res Manage* 2(1):11–24
- 539 Granger D, Fabel D, (2012) Cosmogenic isotope dating of caved-
540 iments. In: *Encyclopedia of Caves (Second Edition)*, pp 172–177
- 541 He J, Xia S, Zeng C, Di Y, Liu M, Lan J, Xiao H, Zhu H, Zeng Q
542 et al (2018) Chemical denudation rate in typical humid
543 subtropical dolomite catchments: a case study in the Huangzhou
544 River basin, Shibing. *Guizhou Earth Environ* 46(3):274–281
- 545 Hill C, Eberz N, Buecher R (2008) A karst connection model for
546 Grand Canyon, Arizona, USA. *Geomorphology* 95:316–334
- 547 Hu Z, Pan B, Guo L, Vandenberghe J, Hu X et al (2016) Rapid fluvial
548 incision and headward erosion by the yellow river along the
549 jinshaan gorge during the past 1.2 ma as a result of tectonic
550 extension. *Quatern Sci Rev* 133:1–14
- 551 Karlstrom K, Lee J, Kelley S, Crow R, Crossey L, Young R, Lazear
552 G, Beard L, Ricketts J, Fox M et al (2014) Formation of the
553 grand canyon 5 to 6 million years ago through integration of
554 older palaeocanyons. *Nat Geosci* 7(3):239–244
- 555 Li X (2001) An analysis of physiographic stage in the karst region of
556 Guizhou Plateau. *Guizhou Geol* 3:182–186
- 557 Liu Y, Wang S, Xu S, Liu X, Fabel D, Zhang X, Luo W, Cheng A
558 et al (2013) New evidence for the incision history of the
559 Liuchong River, Southwest China, from cosmogenic $^{26}\text{Al}/^{10}\text{Be}$
560 burial ages in cave sediments. *J Asian Earth Sci* 73:274–283
- 561 Luo S, Li P, Chen W, WY, Ouyang Z, Qin X et al (2019) Study on
562 development mechanism and evolution of Shuanghe Cave
563 system in Suiyang, Guizhou. *J Chongqing Normal Univ Nat
564 Sci Edition* 36(1):111–118
- 565 Meng Q, Shen H, Mao L, Liang W, Zhao Z, Liang Z, Lai M, Huang
566 B, Li S, He M, Shan J et al (2017) Determination of exposure
567 age of Tiankeng, Leye county of Guangxi by accelerator mass
568 spectrometry. *J Guangxi Normal Univ Nat Sci Edition*
569 35(1):16–20
- 570 Michelena M, Kilian R, Baeza O, Rios F, Rivero M, Mesa J,
571 González V, Ordoñez A, Langlais B, Rocca M, Acevedo R et al
572 (2020) The formation of a giant collapse caprock sinkhole on the
573 Barda Negra plateau basalts (Argentina) Magnetic, mineralogical
574 and morphostructural evidences. *Geomorphology* 367:107297
- 575 Nicod J (1997) The karstic canyons, geomorphological problems and
576 new directions (particularly in mediterranean and tropical lands).
577 *Quaternaire* 8(2):71–89
- 578 Piccini L, Drysdale R, Heijnis H (2003) Karst morphology and cave
579 sediments as indicators of the uplift history in the Alpi Apuane
580 (Tuscany, Italy). *Quatern Int* 101–102:219–227
- 581 Polyak V, Hill C, Asmerom Y (2008) Age and evolution of the Grand
582 Canyon revealed by U-Pb dating of water table-type spe-
583 leothems. *Science* 319:1377–1380
- 584 Sasowsky ID (1998) Determining the age of what is not there. *Science*
585 279(5358):1874
- 586 Shen C, Edwards R, Cheng H, Dorale J, Thomas R, Moran S,
587 Weinstein S, Edmonds H et al (2002) Uranium and thorium
588 isotopic and concentration measurements by magnetic sector
589 inductively coupled plasma mass spectrometry. *Chem Geol*
590 185(3–4):165–178

- 592 Shui W, Chen Y, Wang Y, Su Z, Zhang S et al (2015) Origination, study progress and prospect of Karst Tiankeng research in China. Acta Geogr Sin 70(3):431–446 615
- 593 616
- 594 617
- 595 Sweeting M (1995) Karst in China. Its Geomorphology and Environment/Springer V. pp: 265 618
- 596 619
- 597 Szczygiel J, Golicz M, Hercman H, Lynch E et al (2018) Geological constraints on cave development in the plateau- gorge karst of south china (wulong, chongqing). Geomorphology 304:50–63 620
- 598 621
- 599 622
- 600 Tapponnier P (2001) Oblique stepwise rise and growth of the tibet plateau. Science 294(5547):1671–1677 623
- 601 624
- 602 Telbisz T, Stergiou C, Mindszenty A (2019) Karst features and related social processes in the region of the Vikos gorge and Tymphi mountain (Northern Pindos National Park, Greece). Acta Carsologica 48(1):29–42 625
- 603 626
- 604 627
- 605 628
- 606 Waltham T (2005) Collapse processes at the Tiankengs of Xingwen. Cave and Karst Science 32(2–3):107–110 629
- 607 630
- 608 Waltham T (2015) Large collapse sinkholes, old and new, in the Obruk Plateau, Turkey. Cave Karst Sci 42:125–130 631
- 609 632
- 610 Wang F, Li H, Zhu R, Qin F et al (2004) Late quaternary downcutting rates of the Qianyou River from U/Th speleothem dates, Qinling mountains China. Q Res 62(2):194–200 633
- 611 634
- 612 635
- 613 Wang L, Ma Z, Cheng H, Duan W, Xiao J et al (2016) Determination of ^{230}Th dating age of uranium-series standard sample by multiple collector inductively coupled plasma mass spectrometry. J Chin Mass Spectrometry Soc 37(3):262–272 616
- 614 617
- Wang L, Ma Z, Sun Z, Wang Y, Wang X, Cheng H, Xiao J et al (2017) U concentration and $^{234}\text{U} / ^{238}\text{U}$ of seawater from the Okinawa Trough and Indian Ocean using MC-ICPMS with SEM protocols. Mar Chem 196:71–80 618
- 619 620
- 621 621
- 622 622
- 623 623
- 624 624
- 625 625
- 626 626
- 627 627
- 628 628
- 629 629
- 630 630
- 631 631
- 632 632
- 633 633

UNCORRECTED PROOF

Journal : **11631**

Article : **510**

Author Query Form

Please ensure you fill out your response to the queries raised below and return this form along with your corrections

Dear Author

During the process of typesetting your article, the following queries have arisen. Please check your typeset proof carefully against the queries listed below and mark the necessary changes either directly on the proof/online grid or in the 'Author's response' area provided below

Query	Details Required	Author's Response
AQ1	As keywords are mandatory for this journal, please provide 3–6 keywords.	